Photoinitiator-free multi-photon fabrication of compact optical waveguides in polydimethylsiloxane

GIULIA PANUSA,[1] YE PU,[1,*] JIEPING WANG,[1,2] CHRISTOPHE MOSER,[2] AND DEMETRI PSALTIS[1]

[1]*Optics Laboratory (LO), École Polytechnique Fédérale de Lausanne (EPFL), Lausanne, Switzerland*
[2]*Laboratory of Applied Photonics Devices (LAPD), École Polytechnique Fédérale de Lausanne (EPFL), Lausanne, Switzerland*
*ye.pu@epfl.ch

Abstract: Compact, low loss flexible optical waveguides are crucial in optofluidic and microfluidic devices for a dense integration of optical functionalities. We demonstrate the fabrication of compact optical waveguides in polydimethylsiloxane through multiphoton laser direct writing using phenylacetylene as the photosensitive monomer. Our fabrication technique employs photo-induced radical chain polymerization initiated by the monomer molecule itself without a photoinitiator. Because of the dense π-electrons in phenylacetylene, we achieved a high refractive index contrast ($\Delta n \geq 0.06$) between the waveguide core and the PDMS cladding. This allowed for efficient waveguiding with a core size of 1.3-μm with a measured loss of 0.03 dB/cm in the spectral band of 650-700 nm.

1. Introduction

Polydimethylsiloxane (PDMS) is an elastomer of great technological importance, having excellent elasticity and wide spectral range of transparency [1,2], and outstanding chemical [3] and thermal stability. It is widely used in the fabrication of microfluidic [4] and optofluidic devices in particular [5]. Dense integration of optical and fluidic functionalities becomes increasingly essential, calling for compact, low-loss, three-dimensional (3D) optical waveguides in such devices. Prominent examples include biosensing [6], optogenetics [7–10], microfluidic flow cytometry [11,12], wearable photonics [13], and optical printed circuit boards [14–16]. Figure 1 illustrates an envisioned example PDMS hybrid photonic/fluidic device where 3D optical waveguides in several different configurations and microfluidic channels are tightly integrated.
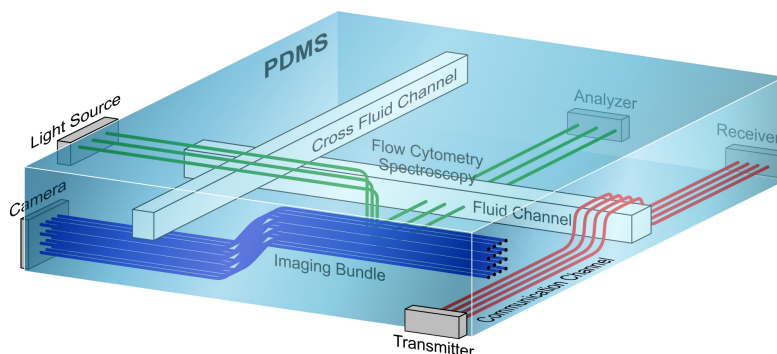

Fig. 1. An envisioned example of 3D optical waveguides integrated in one flexible PDMS substrate with microfluidic channels. Blue wires illustrate an imaging waveguide bundle. Red wires exemplify optical communication channels. Green wires depict optical systems of flow cytometry or spectroscopy.

Femtosecond laser micromachining is a technique for the fabrication of complex structures inside glass and polymer based materials that exploits both additive and subtractive manufacturing strategies [17]. When a high laser intensity is reached inside a medium, nonlinear optical processes occur, one of which is the simultaneous absorption of multiple photons whose combined energy induces a molecular transition that leads to structural modifications in that material. A large number of works have focused on the structural modification through multiphoton laser direct writing (MP-LDW), particularly in dielectric materials. This has led to the development of processes for the fabrication of submicron fine systems, which are suitable for the realization of small photonic devices in glass [18,19], and polymer materials [20,21]. Besides submicron resolution, the nonlinearity of multi-photon absorption also enables the formation of an arbitrary 3D shape within a bulk material.

Optical waveguides are one of the most important photonic components. More specifically, optical waveguides are a key element in the development of multifunctional platforms with tailored geometries, such as biomedical and biosensor platforms. Several techniques aiming at inducing a refractive index change in polymers have been developed. Electro-optic polymers show a change of the refractive index under photo-bleaching from femtosecond laser irradiation [22], and photosensitive resists have been investigated for the realization of stand-alone photonic wire bonding [23]. Because of the versatility of polymers, it is possible to combine standard microfabrication technologies with the advantage of embedding the desired pattern directly into a preformed material, where undoped PMMA is the most commonly used polymer for optical waveguide writing applications [24–26].

PDMS optical waveguides fabrication in a host-guest system has been previously reported [27,28]. When a preformed PDMS substrate is immersed into a high-refractive index liquid monomer formulation, the monomer molecules will permeate into the intermolecular space of the PDMS matrix. Selective photopolymerization of the permeated monomer by a laser focus can induce a local change of the refractive index in the substrate material. Waveguides with a diameter of 50 μm, a refractive index change of $\Delta n \sim 0.01$, and an optical loss between 0.3 and 0.6 dB/cm at a wavelength of 850 nm have been reported [28].

In photopolymerization, the energy of light upon absorption must be transformed into suitable chemical energy in the form of reactive intermediates, a process called photoinitiation. This conversion is usually achieved with a photoinitiator, since light absorption in most monomers is only efficient in deep ultraviolet (DUV) region. A photoinitiator is a compound that produces reactive species upon absorption of light in the designated spectral region. The reactive species then start a chain-growth polymerization by transferring the chemical energy to the monomer molecules. In certain circumstances, however, the addition of photoinitiators increases the chemical complexity of a polymer system. In particular, in biomedical applications where biocompatibility is a prerequisite, a great special design effort is required to ensure that the photoinitiator is nontoxic. Regardless of the biocompatibility of the final polymer product, reducing the chemical complexity by eliminating the photoinitiator would be beneficial in all biomedical applications, particularly implanted devices. Although photoinitiators were ubiquitously used in multiphoton photopolymerization [29–31], ultrafast lasers provide an opportunity to achieve this goal with multiphoton absorption without the use of photoinitiators. Given sufficient laser intensity, the DUV absorption peak of most monomers becomes accessible through two- or three-photon absorption at an appropriate laser wavelength and intensity.

In this work, we demonstrate, for the first time, the fabrication of compact (1.3 μm wide) PDMS optical waveguides through MP-LDW in PDMS without using a photoinitiator. Our characterization shows a high refractive index contrast of $\Delta n \approx 0.06$ and a low transmission loss of 0.03 dB/cm in the 650-700 nm spectral region. We expect our technique to find applications in biosensors, microfluidic flow cytometry, electro-elastic optical modulators, flexible optical circuit boards, wearable and implanted photonic devices, and optical neuron stimulation.

2. Methodology and fabrication process

The host-guest system we describe in this paper includes a PDMS matrix as the host and a liquid monomer permeated into the PDMS intermolecular space as the guest. Besides being polymerizable with good reactivity, requirements on the monomer formulation include: 1. The refractive index of the monomer must be higher than that of the PDMS host matrix; 2. The monomer molecule must be small and nonpolar to allow for a high solubility in PDMS and an easy extraction after laser exposure. 3. The absorption spectrum of the monomer must not overlap with the PDMS host. The first requirement generally necessitate π-electron rich phenyl group in the monomer formulation. Acrylate group, one of the most reactive polymerizable group, fails to meet the second requirement due to its slight polar nature and poor solubility in PDMS. The third requirement is usually satisfied in most nonpolar small-molecule monomer formulations. Based on these considerations, we identified styrene and phenylacetylene as the best candidates. Despite being a widely used building block for polymers, styrene did not show meaningful polymerization without a photoinitiator in our tests. Phenylacetylene, on the other hand, readily achieves photoinitiator-free multiphoton polymerization in PDMS, which is in consistency with the heuristics from previous studies in multiphoton photoinitiators [31].

In this work, we fabricate poly(phenylacetylene) waveguides in platinum-cured PDMS slabs, since it is the only form of PDMS that is medically approved and suits many of our target applications. Condensation cured PDMS should also work in a similar fashion, although we did not test it specifically. Our fabrication technique (Fig. 2) employs photo-induced radical chain polymerization initiated by the phenylacetylene monomer molecule itself without a photoinitiator [Fig. 2 (f)]. The fabrication procedure of the waveguides consists of four steps [Fig. 2(a)-(d)]: 1. the preparation of a pristine platinum-cured PDMS slab (NuSil MED 6215); 2. the permeation of the monomer into the PDMS matrix by immersing the PDMS slab in the phenylacetylene liquid formulation (used as purchased from Sigma Aldrich) for 24 hours [27] [32] to ensure the concentration of phenylacetylene in the PDMS slab reaches the saturation point, after which the PDMS slab gains more than 40% in weight; 3. the exposure of the monomer-permeated PDMS slab to a focused ultrashort laser irradiation to induce polymerization of phenylacetylene and form waveguide structures; and 4. the removal of the unreacted monomer through an ethanol washing followed by a heating step at 100-130 °C for two hours. Figure 2(e) shows the UV absorption spectrum measured with a UV-visible spectrophotometer (Cary 100), which reveals an absorption peak in the spectral range of 215-250 nm. The reaction scheme of the multiphoton polymerization is illustrated in the inset in Fig. 2(e).
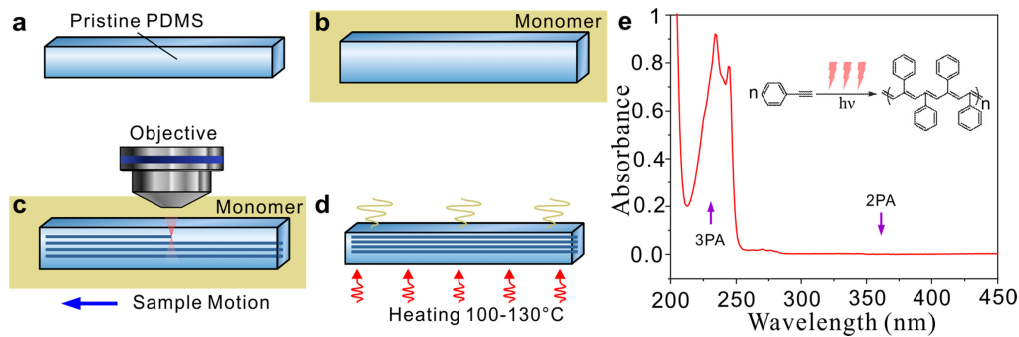
Fig. 2. Principle of waveguides fabrication in PDMS. (a) Preparation of a pristine platinum-cured PDMS substrate. (b) Permeation of the monomer molecules into the PDMS matrix by immersing the PDMS substrate into the monomer liquid formulation for 24 hours. (c) Exposure of the monomer-permeated PDMS substrate to a focused ultrashort laser irradiation for waveguide writing. (d) Removal of the unreacted monomer through an optional ethanol washing and a heating at 100-130 °C for two hours. (e) Absorption spectrum of 0.01 mM phenylacetylene in acetonitrile. Violet arrows indicate energies of two-photon (2PA) and three-photon absorption (3PA). Inset illustrates the reaction of multiphoton polymerization of phenylacetylene, which results in abundant conjugated carbon-carbon double bonds that extend the absorption into the visible blue-green band.

We used a femtosecond Ti:Sapphire laser (Coherent Chameleon Ultra II, 80 MHz repetition rate, 140 fs pulse width) tuned to 680 nm, which allowed for efficient initiation of polymerization reaction through multi-photon absorption in phenylacetylene molecules. The laser beam was focused with a long-working distance, water-immersion objective (0.7 NA) into the PDMS slab (set-up schematic in Fig. 3). Considering an average laser power at the level of 60 mW, 680 nm wavelength source and 0.7 NA lens, we estimate that the focal intensity, ignoring the spherical aberration due to the refractive index mismatch, and the possible self-focusing effect, reaches approximately 2×10^{12} W/cm^2 with fine adjustments by tuning the laser power. The phenylacetylene-permeated PDMS slab sample was sandwiched between a glass microscope slide and a coverslip. To control the depth position of the laser focus, we used a dichroic mirror (50% T/R @650 nm) to steer the full power of the laser beam for writing while allowing a very small amount of leaked laser light reflected from the top surface of the sample cover slip to reach the CMOS camera after a focusing lens. A good focus spot on the camera indicates that the laser is focusing on the top surface of the coverslip, and the consequent control depth is achieved by moving the objective using the translation stage with a micrometer drive.

We wrote waveguides at writing speeds ranging between 0.5 and 1.5 mm/s, at a laser peak intensity between 1.6×10^{12} and 2.4×10^{12} W/cm^2, and at a focusing depth between 800 μm and 1.3 mm below the sample top surface.
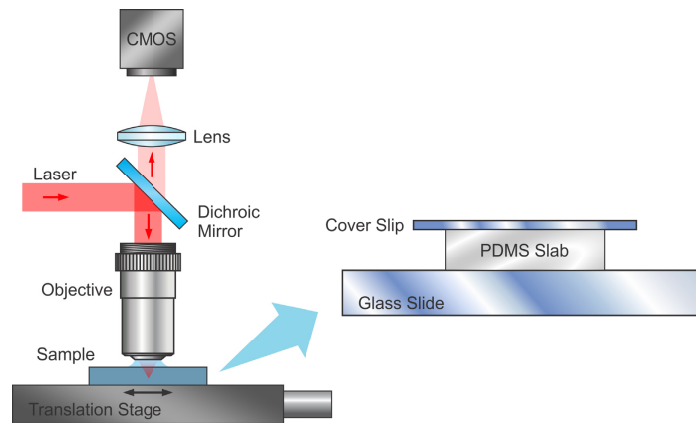
Fig. 3. Experimental set up for waveguide writing in PDMS through MP-LDW. After beam expansion, the full power of the laser beam is steered by the dichroic mirror to the high NA water immersion objective for waveguide writing in the PDMS sample, the structure of which is illustrated in the blowup on the right. A very small amount of leaked laser light reflected from the top surface of the sample coverslip is allowed to reach the CMOS camera after the focusing lens for the control of the focus depth position. The shape of the waveguide being written is controlled by the path of motion set to the stage carrying the sample.

3. Results and discussion

3.1 PDMS waveguides verification

A phase contrast microscope (Nikon IX-71) was used to observe the sample after irradiation, and the phase contrast images clearly reveal the formation of the waveguides. An example phase contrast image of the waveguides is shown in Fig. 4(a), which were fabricated at 1.3 mm depth inside the PDMS material, with 1.9×10^{12} W/cm^2 peak laser intensity and at 0.7 mm/s writing speed. A bright field microscopy image of the waveguide [Fig. 4(b)], obtained using a 1.4 NA oil-immersion objective, reveals a smooth core refractive index structure. The width of the waveguide was measured to be 1.3 µm.
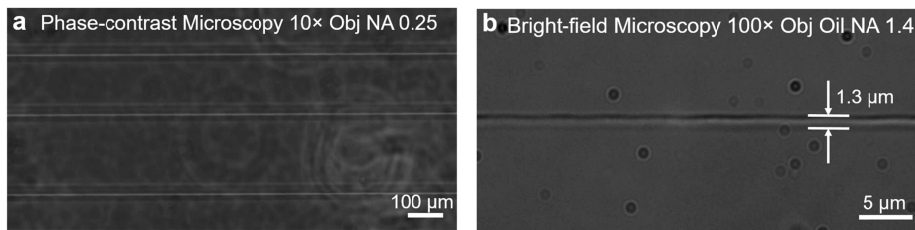

Fig. 4. (a) Phase contrast microscope (Nikon IX-71) image of written PDMS optical waveguides; (b) bright field microscope image of an optical waveguide (60 × magnification objective), written at 1.3 mm below the sample top surface, 1.9×10^{12} W/cm^2 laser peak intensity and 0.7 mm/s writing speed.

The experimental parameters that determine the width of the focal volume, and therefore the resulting feature size, are the pulse energy, the writing speed, and the numerical aperture of the lens used for focusing the beam on the sample. We performed writing experiments in order to characterize the material in terms of polymerization threshold power and writing speed. Figure 5(a) exemplifies the strategy followed to determine the writing power threshold, defined as the minimum laser power for which continuous, sharp and intact polymerized structures are clearly identifiable in our phase contrast microscope. These experiments suggest that the laser peak intensity needed to fabricate a waveguide inside the PDMS slab at the investigated depth is 1.7×10^{12} W/cm^2. This set of experiments was performed at a

writing speed of 0.7 mm/s, which is in the optimal range found experimentally to fabricate undamaged polymerized structures. The cross section of each waveguide has been evaluated by performing a cross-sectional cut and inspecting its core with phase contrast microscopy, as shown in Fig. 5(c).
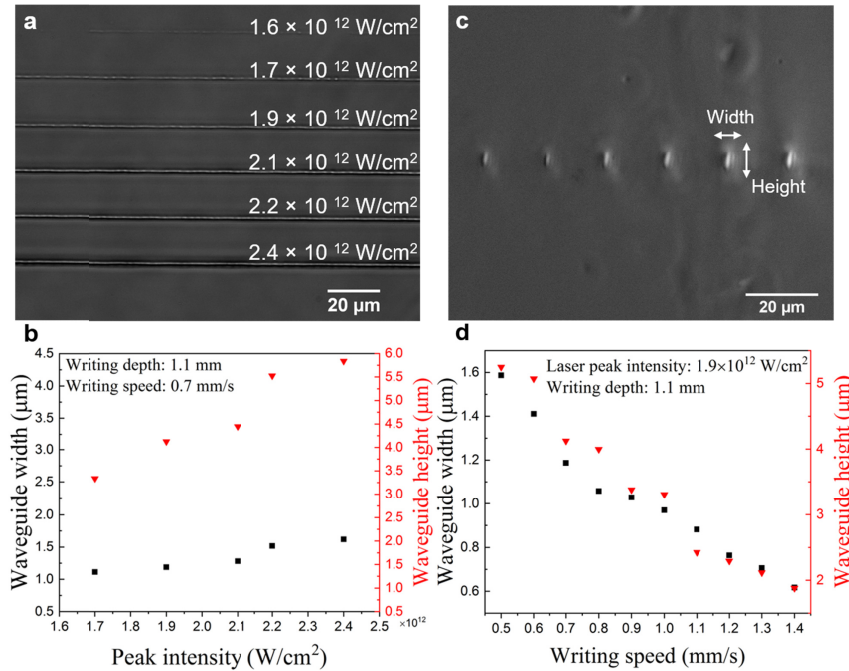

Fig. 5. (a) Top view image and (b) waveguide width and height for optical waveguides written at 0.7 mm/s, 1.1 mm below the sample coverslip interface, for different laser peak intensities; and (c) cross-sectional image and (d) width and height for waveguides written at 1.9 W/cm² peak intensity, 1.1 mm below the sample coverslip interface, for different writing speeds.

Waveguide width and height increase with increasing peak intensity and decreasing writing speed, as revealed in Fig. 5(b) and (d). The aspect ratio, considered as the ratio between waveguide height and waveguide width, ranges from approximately 3.8 at the photopolymerization threshold of 1.7×10^{12} W/cm² to 4.1 at 2.1×10^{12} W/cm². Indeed, the waveguide depth increases at a faster rate compared to its width, resulting in a more elliptical shape at high peak intensities. At constant laser peak intensity and writing depth inside the material, waveguide width and depth decrease linearly with the writing speed, as depicted in Fig. 5 (d).

We also evaluated the impact of the writing depth at fixed writing speed and laser peak intensity on the waveguide cross section [examples are reported in Fig. 6(a), (b) and (c)]. Plot in Fig. 6(d) shows the linear decrease of both lateral and vertical waveguides dimensions with increasing writing depth, as expected considering that a deeper focusing distance corresponds to an increased aberration in the PDMS matrix.
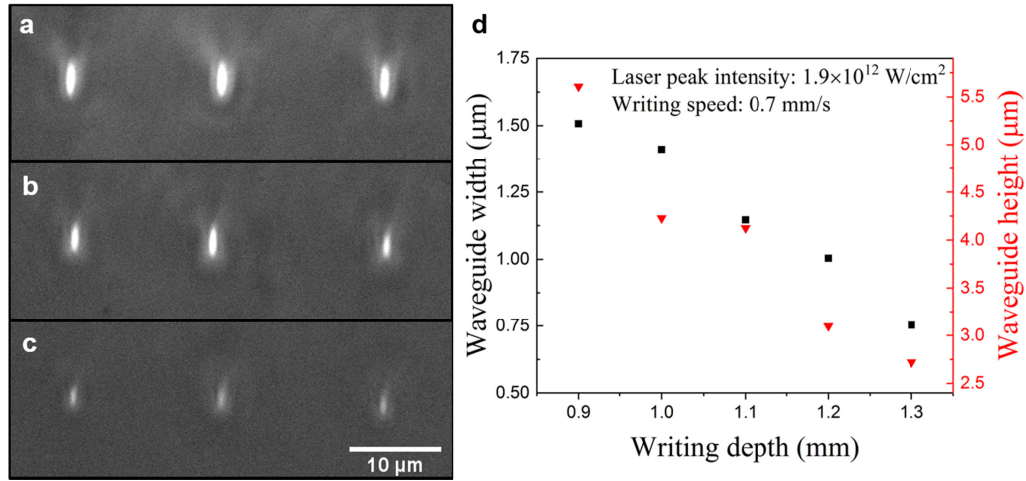
Fig. 6. Waveguide cross section for optical waveguides written at laser peak intensity of 1.9 × 10^{12} W/cm^2 and a writing speed of 0.7 mm/s, for (a) 900 µm, (b) 1.1 mm and (c) 1.3 mm focusing depth; (d) Plot of waveguide width and height as a function of writing depth, showing linear decrease of both lateral and vertical waveguides dimensions with increasing writing depth.

3.2 PDMS waveguides characterization

We characterized the waveguides in terms of refractive index contrast (Δn) and transmission loss. Measurements of the refractive index contrast were performed in a custom made off-axis interferometric imaging system, as illustrated in Fig. 7(a) [33]. The sample is illuminated by a collimated plane wave Helium-Neon (λ = 632.8 nm) laser beam perpendicular to the waveguide, and imaged with a 4f system using a 20 × 0.5 NA objective onto a CMOS camera. A plane-wave reference beam interferes with the waveguide image through a beam splitter, revealing the phase change induced on the illumination beam as it crosses the waveguide. An example interferogram is shown in Fig. 7(b). The average phase change along the waveguide, as shown in Fig. 7(c), is approximately $\Delta\varphi = 1$ rad. Due to the aberration caused by the PDMS layer that the objective wave has to propagate through, the image of the waveguide broadens from 1.3 µm to ~3 µm. We thus estimate the actual phase change to be $\Delta\varphi = 2.3$ rad. Based on the measured height of the waveguide $h \approx 4$ µm and the estimated average phase change, we estimate that the refractive index contrast is $\Delta n = \Delta\varphi\lambda/2\pi h \approx 0.06$ .This implies a polymer content of roughly 35% by mass given the refractive index of 1.59 and 1.41 for poly(phenylacetylene) and PDMS, respectively.

To measure the transmission loss, we coupled thermal white light from a halogen lamp passing a 1-mm iris into the waveguide using a 50 × 0.8 NA objective [Fig. 8(a)] and imaged the output using a digital CMOS camera [Fig. 8(b)]. The iris was imaged on to the incident face of the waveguide as a 17-µm spot with nearly homogeneous intensity. Our motion stage was able to position the waveguide at the center of the incoherent light spot with better than 1 µm accuracy, ensuring the consistency of the coupling condition across multiple mount and dismount of the sample. Taking advantage of this experimental setting, we measured the ratio of the output power from the same waveguides cut into two different lengths. This power ratio reveals the transmission loss due to the material absorption and the scattering loss caused by the waveguide walls smoothness in the polymer waveguide as $\alpha = -\ln\left(P_1/P_2\right)/\left(L_1 - L_2\right)$, where α is the transmission loss in dB/cm, and P_1 and P_2 are the measured output power of the waveguide at lengths L_1 and L_2 .
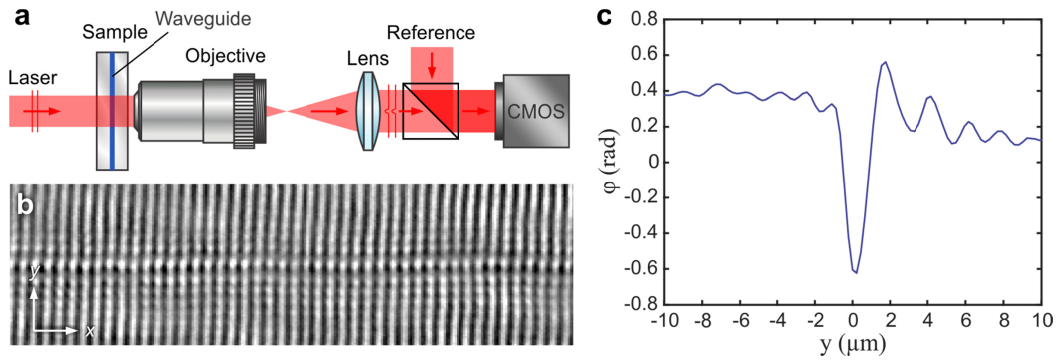
Fig. 7. Measurement of the phase profile and refractive index contrast of the waveguide. (a) Principle of the measurement. A laser beam of plane wave is sent to pass the PDMS sample where the waveguide induces an additional phase change in the wave front, which is measured in the interferometric imaging system. (b) An example interferometric image of the waveguide. Fringes parallel to the waveguide are due to the aberration resulted from the PDMS material. (c) Extracted average phase profile of the waveguide, which is broadened due to the aberration introduced by the PDMS material. The corresponding refractive index contrast, after taking into account the broadening, is $\Delta n \approx 0.06$.
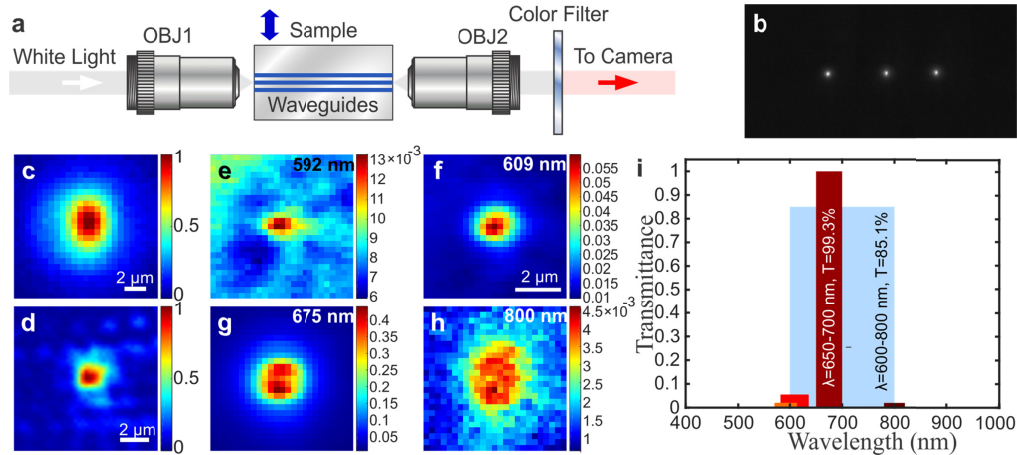

Fig. 8. Characterization of the waveguide transmission. (a) Diagram of the optical set-up used for optical transmission loss characterization. (b) Broadband light output from three individual waveguides written at 800 μm under the top surface, using 1.9×10^{12} W/cm^2 peak intensity and 0.7 mm/s writing speed. (c) Broadband waveguiding output from one waveguide. (d) Laser (HeNe) waveguiding output from the same waveguide. (e) – (h) Filtered narrowband waveguiding output from the same waveguide: (e) 592/43 nm, (f) 675/50 nm, (g) 609/53 nm, and (h) 800/40 nm. (i) Waveguide transmissivity measured by the intensity ratio between the outputs from waveguides cut at different lengths. Light blue, orange, red, brown and black bars show the measured transmissivity at 1 cm in 600 – 800 nm, 570 – 613 nm, 582 – 635 nm, 650 – 700 nm, and 780 – 820 nm, respectively.

We measured the transmission loss using the incoherent thermal source at $L_1 = 16$ mm and $L_2 = 12$ mm. The measured output power of the light source has a statistical coefficient of variation of 1.5% over two hours. Before each measurement, we perform careful adjustments to ensure a consistent output power. Figure 8(c) shows the output from one waveguide when incoherent thermal white light is launched. Additionally, we also launched laser light of 633 nm wavelength into the waveguide, the output of which is shown in Fig. 8(d). The mode field diameter of approximately 2 μm at this wavelength is consistent with the refractive index contrast of 0.06. With the incoherent light, we measured a transmission loss of 6 dB/cm over the entire white light spectrum; however, measurements with color filters

suggested that the absorption loss is highly chromatic, as shown in Fig. 8(e) – (h). The transmissivity measured using a long pass filter cut at 532 nm is 85% at 1 cm length, corresponding to a loss of 0.7 dB/cm. Three waveguides were measured with a standard deviation of 0.07% in the transmissivity, confirming the consistency of the measurements and the waveguide property. Furthermore, the transmissivity measured at 592 nm and 800 nm using band pass filters of 40 nm bandwidth is nearly zero [orange and black bars in Fig. 8(i), respectively], suggesting that the 85% transmission is mainly located in the 600 – 800 nm wavelength range, as shown in Fig. 8(i) (light blue bar). In particular, within a narrower band of 650-700 nm, the measured transmissivity becomes 99.3% at 1 cm length, corresponding to a transmission loss of 0.03 dB/cm, as shown in Fig. 8(i) (dark red bar).

4. Discussion

Due to the high peak intensity at the focus, nonlinear self-focusing is expected to play a role in the high aspect ratio of the waveguide and the occasional spots of material damage. Previous reports have shown that the nonlinear refractive index of electronic origin in poly(phenylacetylene) is on the order of $2.8 \times 10^{-14} cm^2/W$ [34], which leads to a critical power for self-focusing on the order of 1.5×10^4 W. Furthermore, the concentration of the photo-induced polymer, and thus the refractive index of the region concerned, is a power function of the laser intensity. This gives an additional intensity-dependent refractive index contribution of a chemical origin with a response time possibly at the level of ms. The quantification of this chemical contribution is beyond the scope of this paper, although we expect it to be much greater than the electronic contribution. The writing peak power used in our system, on the other hand, was around 5.4×10^3 W, which is below the critical power for self-focusing by electronic contribution but very probably above the critical power for self-focusing by chemical contribution. Therefore, material damages always take place when the writing speed is low due to uncontrollable beam collapse. At optimal writing speed, the polymerization tends to grow along the depth direction, causing an elongated shape in the fabricated waveguides, but beam collapse does not happen due to the slow response time of the reaction.

5. Conclusions

We have demonstrated that compact optical waveguides can be fabricated in PDMS through multi-photon laser direct writing and photopolymerization. We achieved for the first time photoinitiator-free polymerization by tuning the writing laser wavelength to 680 nm such that the absorption band of the monomer is reached via multi-photon absorption. The fabricated waveguides we characterized are approximately 1.3 μm wide with $\Delta n \geq 0.06$ and a transmission loss of 0.03 dB/cm in the spectral range of 650 – 700 nm. We expect such waveguides will receive a wide range of applications in biosensors, microfluidic flow cytometry, wearable photonic devices, electro-elastic optical modulators, flexible optical circuit boards, and optical neural networks.

Funding

References

1. F. Schneider, T. Fellner, J. Wilde, and U. Wallrabe, "Mechanical properties of silicones for MEMS," J. Micromech. Microeng. **18**(6), 065008 (2008).
2. F. Schneider, J. Draheim, R. Kamberger, and U. Wallrabe, "Process and material properties of polydimethylsiloxane (PDMS) for Optical MEMS," Sens. Actuators A Phys. **151**(2), 95–99 (2009).
3. A. Mata, A. J. Fleischman, and S. Roy, "Characterization of polydimethylsiloxane (PDMS) properties for biomedical micro/nanosystems," Biomed. Microdevices **7**(4), 281–293 (2005).
4. K. B. Mogensen, J. El-Ali, A. Wolff, and J. P. Kutter, "Integration of polymer waveguides for optical detection in microfabricated chemical analysis systems," Appl. Opt. **42**(19), 4072–4079 (2003).

5. W. Song, A. E. Vasdekis, and D. Psaltis, "Elastomer based tunable optofluidic devices," Lab Chip **12**(19), 3590–3597 (2012).
6. F. Prieto, B. Sepúlveda, A. Calle, A. Llobera, C. Domínguez, A. Abad, A. Montoya, and L. M. Lechuga, "An integrated optical interferometric nanodevice based on silicon technology for biosensor applications," Nanotechnology **14**(8), 907–912 (2003).
7. K. Y. Kwon, H.-M. Lee, M. Ghovanloo, A. Weber, and W. Li, "Design, fabrication, and packaging of an integrated, wirelessly-powered optrode array for optogenetics application," Front. Syst. Neurosci. **9**, 69 (2015).
8. F. Pisanello, L. Sileo, I. A. Oldenburg, M. Pisanello, L. Martiradonna, J. A. Assad, B. L. Sabatini, and M. De Vittorio, "Multipoint-emitting optical fibers for spatially addressable in vivo optogenetics," Neuron **82**(6), 1245–1254 (2014).
9. Y. Son, H. J. Lee, J. Kim, H. Shin, N. Choi, C. J. Lee, E.-S. Yoon, E. Yoon, K. D. Wise, T. G. Kim, and I.-J. Cho, "In vivo optical modulation of neural signals using monolithically integrated two-dimensional neural probe arrays," Sci. Rep. **5**(1), 15466 (2015).
10. A. N. Zorzos, J. Scholvin, E. S. Boyden, and C. G. Fonstad, "Three-dimensional multiwaveguide probe array for light delivery to distributed brain circuits," Opt. Lett. **37**(23), 4841–4843 (2012).
11. Z. Wang, J. El-Ali, M. Engelund, T. Gotsaed, I. R. Perch-Nielsen, K. B. Mogensen, D. Snakenborg, J. P. Kutter, and A. Wolff, "Measurements of scattered light on a microchip flow cytometer with integrated polymer based optical elements," Lab Chip **4**(4), 372–377 (2004).
12. M. Kim, D. J. Hwang, H. Jeon, K. Hiromatsu, and C. P. Grigoropoulos, "Single cell detection using a glass-based optofluidic device fabricated by femtosecond laser pulses," Lab Chip **9**(2), 311–318 (2009).
13. W. Zeng, L. Shu, Q. Li, S. Chen, F. Wang, and X.-M. Tao, "Fiber-based wearable electronics: a review of materials, fabrication, devices, and applications," Adv. Mater. **26**(31), 5310–5336 (2014).
14. K. Soma and T. Ishigure, "Fabrication of a graded-index circular-core polymer parallel optical waveguide using a microdispenser for a high-density optical printed circuit board," IEEE J. Sel. Top. Quantum Electron. **19**(2), 3600310 (2013).
15. R. Dangel, C. Berger, R. Beyeler, L. Dellmann, M. Gmur, R. Hamelin, F. Horst, T. Lamprecht, T. Morf, S. Oggioni, M. Spreafico, and B. J. Offrein, "Polymer-waveguide-based board-level optical interconnect technology for datacom applications," IEEE Trans. Adv. Packag. **31**(4), 759–767 (2008).
16. C. Choi, L. Lin, Y. Liu, J. Choi, L. Wang, D. Haas, J. Magera, and R. T. Chen, "Flexible optical waveguide film fabrications and optoelectronic devices integration for fully embedded board-level optical interconnects," J. Lightwave Technol. **22**(9), 2168–2176 (2004).
17. R. R. Gattass and E. Mazur, "Femtosecond laser micromachining in transparent materials," Nat. Photonics **2**(4), 219–225 (2008).
18. F. Chen and J. R. V. de Aldana, "Optical waveguides in crystalline dielectric materials produced by femtosecond-laser micromachining," Laser Photonics Rev. **8**(2), 251–275 (2014).
19. S. Gross, N. Riesen, J. D. Love, and M. J. Withford, "Three-dimensional ultra-broadband integrated tapered mode multiplexers," Laser Photonics Rev. **8**(5), L81–L85 (2014).
20. R. Martínez Vázquez, S. M. Eaton, R. Ramponi, G. Cerullo, and R. Osellame, "Fabrication of binary Fresnel lenses in PMMA by femtosecond laser micromachining," in *CLEO:2011 - Laser Applications to Photonic Applications*, OSA Technical Digest (CD) (Optical Society of America, 2011), JMG5.
21. S. M. Eaton, L. Criante, S. L. Turco, S. S. K. Guduru, and R. Ramponi, "Focused femtosecond laser pulses: A versatile tool for three-dimensional writing of micro-nano devices," in *2014 16th International Conference on Transparent Optical Networks (ICTON)*, 2014), 1–4.
22. B. Amirsolaimani, O. D. Herrera, R. Himmelhuber, K. Kieu, R. A. Norwood, and N. Peyghambarian, "Electro-optic polymer channel waveguide fabrication using multiphoton direct laser writing," in *2015 IEEE Optical Interconnects Conference (OI)*, 2015), 104–105.
23. N. Lindenmann, G. Balthasar, D. Hillerkuss, R. Schmogrow, M. Jordan, J. Leuthold, W. Freude, and C. Koos, "Photonic wire bonding: a novel concept for chip-scale interconnects," Opt. Express **20**(16), 17667–17677 (2012).
24. A. Baum, P. J. Scully, W. Perrie, D. Liu, and V. Lucarini, "Mechanisms of femtosecond laser-induced refractive index modification of poly(methyl methacrylate)," J. Opt. Soc. Am. B **27**(1), 107–111 (2010).
25. W. M. Pätzold, C. Reinhardt, A. Demircan, and U. Morgner, "Cascaded-focus laser writing of low-loss waveguides in polymers," Opt. Lett. **41**(6), 1269–1272 (2016).
26. W. M. Pätzold, A. Demircan, and U. Morgner, "Low-loss curved waveguides in polymers written with a femtosecond laser," Opt. Express **25**(1), 263–270 (2017).
27. R. Infuehr, N. Pucher, C. Heller, H. Lichtenegger, R. Liska, V. Schmidt, L. Kuna, A. Haase, and J. Stampfl, *Functional polymers by two-photon 3D lithography* (2007), Vol. 254, pp. 836–840.
28. R. Woods, S. Feldbacher, D. Zidar, G. Langer, V. Satzinger, V. Schmidt, N. Pucher, R. Liska, and W. Kern, "3D optical waveguides produced by two photon photopolymerisation of a flexible silanol terminated polysiloxane containing acrylate functional groups," Opt. Mater. Express **4**(3), 486–498 (2014).
29. K. J Schafer, J. Hales, M. Balu, K. Belfield, E. Van Stryland, and D. J Hagan, *Two-photon absorption cross-sections of common photoinitiators* (2004), Vol. 162, pp. 497–502.
30. N. Pucher, A. Rosspeintner, V. Satzinger, V. Schmidt, G. Gescheidt, J. Stampfl, and R. Liska, *Structure–Activity Relationship in D-π-A-π-D-Based Photoinitiators for the Two-Photon-Induced Photopolymerization Process* (2009), Vol. 42, pp. 6519–6528.

31. R. Liska and B. Seidl, "1,5-Diphenyl-1,4-diyn-3-one: A highly efficient photoinitiator," J. Polym. Sci. A Polym. Chem. **43**(1), 101–111 (2005).
32. J. N. Lee, C. Park, and G. M. Whitesides, "Solvent compatibility of poly(dimethylsiloxane)-based microfluidic devices," Anal. Chem. **75**(23), 6544–6554 (2003).
33. J. W. Goodman, ed., *Introduction to Fourier Optics,* Third ed. (Ben Roberts, 2005).
34. D. Neher, A. Wolf, C. Bubeck, and G. Wegner, "Third-harmonic generation in polyphenylacetylene: Exact determination of nonlinear optical susceptibilities in ultrathin films," Chem. Phys. Lett. **163**(2-3), 116–122 (1989).